

**Spatial distribution of tunnel current and application to scanning-tunneling microscopy:  
A semiclassical treatment**

Balaram Das\*

*Department of Mathematics, University of Melbourne, Parkville, VIC. 3052, Australia*

J. Mahanty

*Department of Theoretical Physics, Research School of Physical Sciences, The Australian National University,  
Canberra, A.C.T. 2601, Australia*

(Received 27 February 1987)

The Wentzel-Kramers-Brillouin approximation is extended to consider tunneling through three-dimensional potential barriers. The formalism is used to obtain the tunnel-current density in a scanning-tunneling microscope with a realistic model of the potential barrier. It is shown that the tunnel-current density has a sharp peak under the tip, and that explains the high lateral resolution of the instrument.

**I. INTRODUCTION**

The recent development of the scanning-tunneling microscope (STM)<sup>1,2</sup> has stimulated renewed interest in the problem of a particle tunneling through a potential barrier. The high lateral resolution of STM is a consequence of the localization of the tunnel current in the immediate neighborhood of the tip within a region whose lateral dimension is smaller than the radius of curvature of the tip. Our object here is to analyze the problem using the semiclassical method, and demonstrate the extent of localization achieved in a typical STM geometry.

There is an extensive literature on the use of the semiclassical method in multidimensional tunneling problems, which occur in nuclear physics<sup>3</sup> and in molecular physics.<sup>3-6</sup> An application of tunneling through axisymmetric potential barriers of the sort occurring in STM geometry has been given by Sumetskii.<sup>7</sup> The directness of the semiclassical method when applied to such problems is an advantage over the more exact quantum-mechanical treatment. Its lack of exactness is amply compensated by the physical insight it gives, and the results obtained are correct in a semiquantitative sense. In Sec. II we shall briefly outline the use of the method, and in Sec. III we shall discuss its applicability in tunneling problems. Section IV will give the application to STM geometry and Sec. V will conclude the paper.

**II. THE SEMICLASSICAL METHOD**

The basis of the semiclassical method, which reduces to the Wentzel-Kramers-Brillouin (WKB) approximation in one-dimensional problems, is the representation of the wave function  $\psi$  of the tunneling particle of mass  $m$  in the form<sup>8</sup>

$$\psi = \exp \left[ \frac{i}{\hbar} [\sigma(\mathbf{r}) - Et] \right], \tag{2.1}$$

where  $\sigma(\mathbf{r})$  satisfies the equation (obtained from the Schrödinger equation for  $\psi$ )

$$(\nabla\sigma)^2 - i\hbar\nabla^2\sigma = 2m[E - V(\mathbf{r})]. \tag{2.2}$$

Here  $E$  and  $V$ , respectively, are the total energy and the potential energy of the particle. The semiclassical method consists of expanding  $\sigma$  in a power series in  $\hbar$ ,

$$\sigma = \sigma_0 + \left[ \frac{\hbar}{i} \right] \sigma_1 + \left[ \frac{\hbar}{i} \right]^2 \sigma_2 + \dots, \tag{2.3}$$

and evaluating  $\sigma$  to the desired order in  $\hbar$ . The equations that  $\sigma_0$  and  $\sigma_1$  satisfy are

$$(\nabla\sigma_0)^2 = 2m[E - V(\mathbf{r})], \tag{2.4}$$

$$(\nabla\sigma_1 \cdot \nabla\sigma_0) = \frac{1}{2}\nabla^2\sigma_0. \tag{2.5}$$

$\sigma_0$  satisfies the same equation as the one for the characteristic function  $W$  in Hamilton-Jacobi theory in classical mechanics. The Hamilton-Jacobi equation has no significance in the inaccessible region in which  $E < V(\mathbf{r})$ , but in quantum theory  $\psi$  can be built from the complex solution of (2.4) in the inaccessible region, leading to a nonzero probability of the particle being in that region. The method of obtaining a solution of (2.4) in the classically inaccessible region in multidimensional problems has been discussed widely since the classic paper of Kapur and Peierls.<sup>9</sup>

The formal solution of (2.4) is

$$\sigma_0(\mathbf{r}) = \sigma_0(\mathbf{r}_0) + \int_{s_0}^s ds \sqrt{2m[E - V(\mathbf{r})]}, \tag{2.6}$$

where the integration variable  $s$  is the arc length along a ray, i.e., the line of steepest gradient of  $\sigma_0$  on which  $\mathbf{r}_0 \equiv \mathbf{r}(s_0)$  and  $\mathbf{r} \equiv \mathbf{r}(s)$  lie. This ray is a classical trajectory of the particle in the accessible region. In this region  $\mathbf{r}$  can be written parametrically in terms of time  $t$  as

$$\mathbf{r} \equiv \mathbf{r}(t). \tag{2.7}$$

This trajectory is obtained from Newton's equation of motion, or from its first integral,

$$\left(\frac{d\mathbf{r}}{dt}\right)^2 = \frac{2}{m}[E - V(\mathbf{r})], \quad (2.8)$$

using other conservation laws arising out of the symmetry of the potential. Obviously we need a method that would enable us to continue the classical trajectory in the accessible region to a "trajectory" in the inaccessible region, so that  $\sigma_0$  can be calculated in that region from (2.6).

Let  $D$  be the region in which  $V \geq E$ . To simplify the analysis we assume that  $V > E$  in the interior of  $D$  and  $V = E$  on its boundary; this boundary is moreover assumed to be smooth. Clearly, no interior points of  $D$  are accessible along classical trajectories from points outside  $D$ . The boundary of  $D$  on which  $V = E$  is only accessible from points outside  $D$  along those classical trajectories which meet it normally. This is a consequence of the fact that the total kinetic energy of the particle traversing such a trajectory becomes zero at the boundary, and its direction of motion, being along the gradient of  $V$ , is normal to the boundary.

Inside the region  $D$  no classical trajectory is possible for particles having total energy  $E$ . However, a formal trajectory can be constructed by varying the time parameter  $t$  in (2.7) along the imaginary axis<sup>3,6</sup> in the complex  $t$  plane. In other words, a particle with total energy  $E < V(\mathbf{r})$  will have a trajectory inside  $D$  given by the solution of the equation

$$\left(\frac{d\mathbf{r}}{d\tau}\right)^2 = \frac{2}{m}[V(\mathbf{r}) - E], \quad (2.9)$$

obtained from (2.8) by substituting  $t = i\tau$ . Again, this trajectory, where it meets the boundary of  $D$ , does so orthogonally. It is easy to see that this trajectory, which corresponds to "real-time" motion of a particle with the potential  $[-V(\mathbf{r})]$  and total energy  $(-E)$ , will minimize the action in the forbidden region in the way Kapur and Peierls<sup>9</sup> have prescribed. It must be stressed here that the classical trajectory outside  $D$  and its continuation into  $D$  along the solution of (2.9) just gives us the path along which the integral occurring in (2.6) is to be evaluated to help us obtain  $\sigma_0(\mathbf{r})$  when  $\mathbf{r} = \mathbf{r}(s)$  lies inside  $D$ , and that no other significance should be attached to them.

Let us consider a trajectory from a point  $\mathbf{r}_0$  outside the region  $D$ , governed by Eq. (2.8), which meets the boundary at  $\mathbf{r}_1$  (Fig. 1). In this case, if the time increments from the instant the particle was at  $\mathbf{r}_1$  are kept real, the trajectory from  $\mathbf{r}_1$  would retrace itself into the accessible region. If, on the other hand, the time increments are along the imaginary axis, the trajectory from  $\mathbf{r}_1$  will enter the region  $D$ , governed by Eq. (2.9), and may reach the boundary again at  $\mathbf{r}_2$ . It will of course be orthogonal to the boundary at both the entry and exit points. For further imaginary-time increments the trajectory from  $\mathbf{r}_2$  retraces itself into region  $D$ . However, if at the point  $\mathbf{r}_2$  the time increment is made real again, the trajectory from  $\mathbf{r}_2$  will emerge into the classically accessible region as a solution of (2.8).

The various alternatives discussed above give rise to different values of the characteristic function  $\sigma_0$  at any particular point in the trajectory. For example, at a point

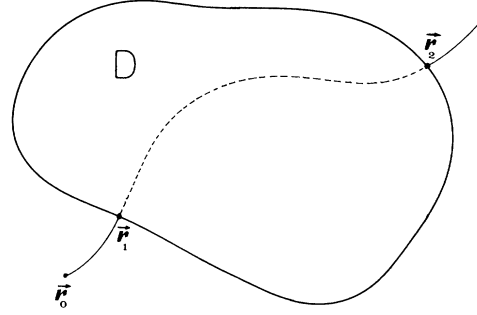


FIG. 1.  $D$  represents the classical inaccessible region where  $E < V$ . A classical trajectory starting at  $\mathbf{r}_0$  in the accessible region meets  $D$  at  $\mathbf{r}_1$  and continues into  $D$  along the solution of (2.9) until it emerges out of  $D$  at  $\mathbf{r}_2$ . From  $\mathbf{r}_2$  onwards it continues as a classical trajectory. The trajectory is normal to  $D$  at  $\mathbf{r}_1$  and  $\mathbf{r}_2$ .

$\mathbf{r}_\alpha$  between  $\mathbf{r}_0$  and  $\mathbf{r}_1$  the characteristic function when evaluated along the trajectory from  $\mathbf{r}_0$  to  $\mathbf{r}_\alpha$  is

$$\sigma_0(\mathbf{r}_\alpha) = \sigma_0(\mathbf{r}_0) + \int_{s_0}^{s_\alpha} \sqrt{2m(E - V)} ds.$$

One can, however, also consider a trajectory which starts from  $\mathbf{r}_0$  and reaches  $\mathbf{r}_\alpha$  after suffering reflection at either or both of the points  $\mathbf{r}_1$  and  $\mathbf{r}_2$ . The characteristic function  $\sigma_0$  when evaluated along such a trajectory will be given by

$$\begin{aligned} \sigma_0^{(n)}(\mathbf{r}_\alpha) = & \sigma_0(\mathbf{r}_0) + \int_{s_0}^{s_1} ds \sqrt{2m(E - V)} \\ & + i2n \int_{s_1}^{s_2} ds \sqrt{2m(V - E)} \\ & - \int_{s_1}^{s_\alpha} ds \sqrt{2m(E - V)}, \end{aligned} \quad (2.10)$$

where  $s_i$  is the value of  $s$  at  $\mathbf{r}_i$ ,  $i=0,1,2,\alpha$  and  $n$  ( $=0,1,2,\dots$ ) is the number of reflections the trajectory suffers at the point  $\mathbf{r}_2$ . Similarly, at a point  $\mathbf{r}_\beta$  on the trajectory beyond  $\mathbf{r}_2$  the characteristic function will be given by

$$\begin{aligned} \sigma_0^{(n)}(\mathbf{r}_\beta) = & \sigma_0(\mathbf{r}_0) + \int_{s_0}^{s_1} ds \sqrt{2m(E - V)} \\ & + i(2n + 1) \int_{s_1}^{s_2} ds \sqrt{2m(V - E)} \\ & + \int_{s_2}^{s_\beta} ds \sqrt{2m(E - V)}. \end{aligned} \quad (2.11)$$

Here  $n$  ( $=0,1,2,\dots$ ) denotes the number of reflections that the trajectory suffers at the point  $\mathbf{r}_1$ .

The time-independent part of the wave function  $\Psi$  at the points  $\mathbf{r}_\alpha$  and  $\mathbf{r}_\beta$  are then given, respectively, as

$$\begin{aligned} \Psi(\mathbf{r}_\alpha) = & A_0 \exp \left[ \frac{i}{\hbar} \left[ \sigma_0(\mathbf{r}_0) + \int_{s_0}^{s_\alpha} \sqrt{2m(E - V)} ds \right] \right] \\ & + \sum_{n=0}^{\infty} A_{n+1} \exp \left[ \frac{i}{\hbar} \sigma_0^{(n)}(\mathbf{r}_\alpha) \right], \end{aligned} \quad (2.12a)$$

$$\Psi(\mathbf{r}_\beta) = \sum_{n=0}^{\infty} B_n \exp \left[ \frac{i}{\hbar} \sigma_0^{(n)}(\mathbf{r}_\beta) \right]. \quad (2.12b)$$

Here we have replaced  $\sigma$  by  $\sigma_0$ ; in other words, we retain only the terms of zeroth order in  $\hbar$  in the expansion (2.3). In these equations the maximum contribution to  $\Psi$  will come from those values of the characteristic function  $\sigma_0$  (at the points  $\mathbf{r}_\alpha$  and  $\mathbf{r}_\beta$ ) which are obtained by integrating Eq. (2.6) along trajectories which do not suffer any reflections at  $\mathbf{r}_1$  or  $\mathbf{r}_2$ . This follows from the fact that when  $n$  changes by 1, the amplitude of the corresponding term in  $\Psi$  in (2.12) diminishes by the exponential factor

$$\exp \left[ -\frac{2}{\hbar} \int_{s_1}^{s_2} ds \sqrt{2m(V-E)} \right].$$

Hence we shall consider the wave functions in the following simpler forms:

$$\Psi(\mathbf{r}_\alpha) = \exp \left[ \frac{i}{\hbar} \left( \sigma_0(\mathbf{r}_0) + \int_{s_0}^{s_\alpha} ds \sqrt{2m(E-V)} \right) \right], \quad (2.13a)$$

$$\begin{aligned} \Psi(\mathbf{r}_\beta) = \exp \left[ \frac{i}{\hbar} \left( \sigma_0(\mathbf{r}_0) + \int_{s_0}^{s_1} ds \sqrt{2m(E-V)} \right. \right. \\ \left. \left. + i \int_{s_1}^{s_2} ds \sqrt{2m(V-E)} \right. \right. \\ \left. \left. + \int_{s_2}^{s_\beta} ds \sqrt{2m(E-V)} \right) \right]. \quad (2.13b) \end{aligned}$$

We shall now proceed to use these wave functions for evaluation of the tunneling current.

### III. THE TUNNELING CURRENT

To obtain the probability current transmissions coefficient in tunneling across the region  $D$ , we consider the set of all trajectories that enter  $D$  and emerge out of it. We give an orientation to this set by specifying that the direction along which the arc-length parameter  $s$  increases along a trajectory is nearly the same as that in nearby trajectories. Each trajectory will have three parts. Part I is the portion of the trajectory before it enters  $D$ , part II is the portion inside  $D$ , and part III is that after it emerges out of  $D$ . Using the form of the wave function given in (2.13), it is easily shown that the probability current density vector  $[\mathbf{J}(\mathbf{r}) = (\hbar/m) \text{Im}(\Psi^* \nabla \Psi)]$  at any point  $\mathbf{r}$  on part I of a trajectory is given by

$$\mathbf{J}_I(\mathbf{r}) = \left[ \frac{2}{m} [E - V(\mathbf{r})] \right]^{1/2} \hat{\mathbf{t}}(\mathbf{r}), \quad (3.1a)$$

and the corresponding expression for the probability current in part III is

$$\mathbf{J}_{III}(\mathbf{r}) = \left[ \frac{2}{m} [E - V(\mathbf{r})] \right]^{1/2} \exp(-T_{12}) \hat{\mathbf{t}}(\mathbf{r}). \quad (3.1b)$$

Here  $\hat{\mathbf{t}}(\mathbf{r})$  is the unit vector along the tangent to the trajectory at  $\mathbf{r}$  and

$$T_{12} = \frac{2}{\hbar} \int_{s_1}^{s_2} ds \sqrt{2m[V(\mathbf{r}) - E]}, \quad (3.2)$$

the integration being along part II of the trajectory, and  $(s_1 - s_2)$  is the corresponding arc length. Therefore, along every trajectory that enters and emerges out of  $D$ , the transmission coefficient, in terms of the ratio of the emerging and entering current densities, is given by

$$T = \left[ \frac{|dV(\mathbf{r})/ds|_{s=s_2}}{|dV(\mathbf{r})/ds|_{s=s_1}} \right]^{1/2} \exp(-T_{12}). \quad (3.3)$$

This coefficient determines the contribution of a trajectory to the tunneling current across  $D$ . This is clearly of the same form as the tunneling transmission coefficient in a one-dimensional problem obtained by WKB approximation.<sup>10</sup> If we take into account multiple reflections at  $\mathbf{r}_1$  and  $\mathbf{r}_2$  and use the wave functions in the form (2.12), the transmission coefficient along a trajectory will turn out to be of the same form as that in a one-dimensional potential-barrier problem. Moreover, the coefficient of reflection along the trajectory will be given by  $R = 1 - T$ . In fact, the three-dimensional tunneling problem is reduced to a one-dimensional tunneling problem along each trajectory.

Trajectories that are close to each other form a tube across the region  $D$  in the same manner as the stream lines in fluid flow form the stream tube. The tunneling current through each such tube (of small cross section) increases with that of the density of the trajectories through the tube and decreases exponentially when the average value of the integral  $T_{12}$  inside the tube increases. These factors can lead to an appreciable localization of the tunneling current through some regions of  $D$ , thereby showing a focusing effect.

### IV. A MODEL FOR STM

In this section a particular model for STM geometry is chosen for illustration. We apply the methods developed in Sec. II to this model and then show the localization of the tunnel current as discussed in the last section. This in turn enables us to have an estimate of the lateral resolution of the STM.

The model has the following essential features. The scanning needle tip is a sphere of diameter  $2a$ . The surface of the sample being investigated is a plane  $(\rho, \theta, z)$  denotes a system of cylindrical coordinates as shown in Fig. 2. The  $(\rho, \theta)$  plane is the sample surface, the  $z$  axis passing through the center of the sphere representing the tip, and  $z_0$  is the distance between the tip and the sample surface. The model having cylindrical symmetry about the  $z$  axis, it is sufficient to take only the  $(\rho, z)$  plane into account to analyze the current distribution.

The potential energy of an electron between the needle tip and the sample surface in this model is taken to be of the form

$$V(\rho, z) = -V_0 \left[ \frac{a}{4z} + \frac{a^2}{2[(z_0 - z + a)^2 + \rho^2 - a^2]} \right].$$

This is very similar to the more exact forms evaluated by Mahanty and Michalewicz.<sup>11</sup> Writing  $x = (z/a)$ ,  $r = (\rho/a)$ , and  $x_0 = (z_0/a)$ , the dimensionless potential energy (with  $V_0 = e^2/a$ ) is given by

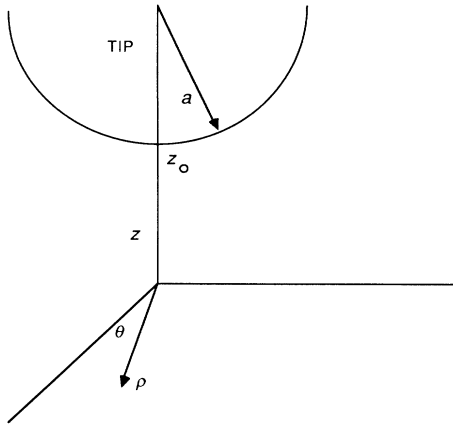


FIG. 2. Essential features of STM geometry.  $(\rho, \theta, z)$  denotes a cylindrical coordinate system, with the  $(\rho, \theta)$  plane being the sample surface, and the  $z$  axis passing through the center of the sphere of radius  $a$  representing the scanning needle tip.  $z_0$  is the distance of the tip from the sample surface.  $a = z_0 = 5 \text{ \AA}$ .

$$\frac{V}{V_0} = - \left[ \frac{1}{4x} + \frac{1}{2[(x_0 - x)^2 + 2(x_0 - x) + r^2]} \right]. \quad (4.1)$$

The surfaces  $E = V$  (for negative  $E$ ) are then given by the solutions of the equation

$$\beta = \frac{1}{4x} + \frac{1}{2[(x_0 - x)^2 + 2(x_0 - x) + r^2]}, \quad (4.2)$$

where  $\beta = |E|/V_0$ . For small values of  $x$  and  $r$ , and  $\beta$  large compared with  $x_0$ , (4.2) has an approximate solution

$$x \approx \frac{1}{4 \left[ \beta - \frac{1}{2(x_0^2 + 2x_0)} \right]}. \quad (4.3)$$

This is a plane close to the sample surface and parallel to it. For  $x$  approaching  $x_0$  from below, (4.2) has a solution

$$[x - (1 + x_0)]^2 + r^2 \approx 1 + \frac{2x_0}{4\beta x_0 - 1}. \quad (4.4)$$

This is a sphere concentric with that representing the tip and has the radius

$$\left[ 1 + \frac{2x_0}{4\beta x_0 - 1} \right]^{1/2}.$$

We consider tunneling across the region  $D$  bound by the two surfaces (4.3) and (4.4).

To obtain the tunneling current we have to evaluate the integral (3.2) along a path across  $D$  governed by the equations

$$m \frac{d^2x}{d\tau^2} = \frac{\partial V}{\partial x}, \quad m \frac{d^2r}{d\tau^2} = \frac{\partial V}{\partial r}. \quad (4.5)$$

Here  $m$  is the mass of the electron. Eliminating  $\tau$  in (4.5) we have

$$\frac{d^2r}{dx^2} = - \frac{1 + \left[ \frac{dr}{dx} \right]^2}{2 \left[ \beta + \frac{V}{V_0} \right]} \left[ \frac{dr}{dx} \frac{\partial(V/V_0)}{\partial x} - \frac{\partial(V/V_0)}{\partial r} \right]. \quad (4.6)$$

Equation (4.6) is solved numerically with the following initial conditions. We choose points  $P_n$ ,  $n = 1, 2, \dots$  along the circumference of the circle (4.4), such that each  $P_n$  has a non-negative  $r$  coordinate and the arc  $P_n P_{n+1}$  subtends an angle of 0.01 rad at the center of the circle. The first point  $P_1$  is the point of intersection of the circle

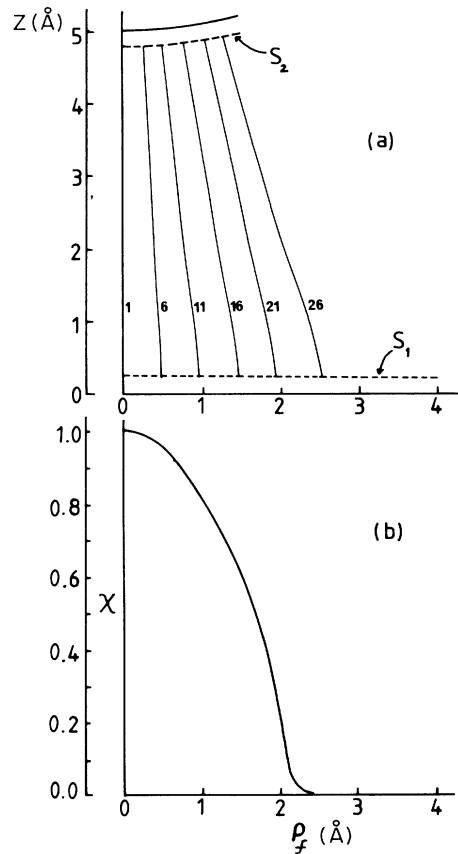


FIG. 3. (a) shows the six trajectories in the region between the tip and the sample surface, referred to in Table I. The number  $n$  of each trajectory is indicated next to it. The dotted lines  $S_1$  and  $S_2$ , representing the equipotential surfaces (4.3) and (4.4), respectively, are the boundaries of the classically inaccessible region  $D$  between them. Six trajectories satisfying (4.5) across  $D$ , each with its initial point on  $S_2$  and final point on  $S_1$ , obtained numerically, are shown. The distances along the  $\rho$  and  $z$  axes are in  $\text{\AA}$ . The tip diameter is  $10 \text{ \AA}$ , and the distance between the tip and the sample surface is  $5 \text{ \AA}$ . (b)  $\rho_f$  denotes the distance in  $\text{\AA}$  along the surface (4.3) from the final point of the axial trajectory.  $\chi$  denotes the ratio of the magnitude of the current density at  $\rho_f$  to that at the final point of the axial trajectory.  $\chi = 0.5$  at  $\rho_f \approx 1.7 \text{ \AA}$ , giving a lateral resolution of the order of  $3.4 \text{ \AA}$ .

TABLE I. The distance from the  $z$  axis of the point of emergence of a trajectory from the potential barrier increases with the trajectory number  $n$ . The  $n$ th trajectory emerges normally from the spherical tip subtending an angle  $(n-1)\times 0.01$  rad with respect to the  $z$  axis. The table shows the increase of  $I_n$  with  $n$ .

Trajectory number $n$	$I_n$
1	1.6518
6	1.6576
11	1.6757
16	1.7127
21	1.9212
26	3.1235

with the  $z$  axis. Since the trajectories governed by (4.5) meet the circle (4.4) orthogonally, the value of  $dr/dx$  at each of the points  $P_n$  is determined. Equation (4.6) is then solved through each of the points  $P_n$  with  $x$  decreasing until the solution curve reaches the surface (4.3). We thus obtain trajectories (4.5) across  $D$ , the  $n$ th trajectory having the initial point  $(x_i, r_i)_n = P_n$  on the surface (4.4) and the final point  $(x_f, r_f)_n$  on the surface (4.3).

Let  $a = \alpha a_0$ ,  $a_0$  being the Bohr radius. Along the  $n$ th trajectory the integral (3.2) becomes

$$(T_{if})_n = 2\sqrt{2\alpha} \int_{(x_i)_n}^{(x_f)_n} dx \left[ \frac{V}{V_0} + \beta \right]^{1/2} \times \left[ 1 + \left( \frac{dr}{dx} \right)^2 \right]^{1/2} \equiv 2\sqrt{2\alpha} I_n. \quad (4.7)$$

We assume that the tunnel-current density has a constant magnitude over the surface of the tip. Then the ratio of  $J_n$ , the magnitude of the current density at the end of the  $n$ th trajectory, to  $J_1$ , the magnitude of the current density at the end of the first trajectory, is given by

$$\chi_n \equiv \frac{J_n}{J_1} = \frac{\gamma_n}{\gamma_1} \exp[2\sqrt{2\alpha}(I_1 - I_n)], \quad (4.8)$$

where

$$\gamma_n = \left[ \frac{|dV/ds|_{s=s_1}}{|dV/ds|_{s=s_i}} \right]^{1/2}$$

on the  $n$ th trajectory.

The trajectories of (4.5) are obtained with parameters  $\beta=5$  and  $x_0=1$ . The integral  $I_n$  is then evaluated along each trajectory with  $2a = 10 \text{ \AA}$ , i.e.,  $\alpha=9.45$ . The results

are plotted in Fig. 3. They demonstrate the following features.

(i) The first trajectory, i.e., the one starting at the point  $P_1$ , is along the  $z$  axis inside the region  $D$ . For other trajectories the ratio  $(\rho_f/\rho_i)$  is a factor greater than unity, and increases with  $n$  [Fig. 3(a)]. In other words, as we approach the plane of the sample surface, the current tubes spread further apart.

(ii) The integral  $I_n$  along a trajectory increases with the distance of the trajectory from the  $z$  axis (Table I). Hence the transmission ratio  $T$  of (3.3) along a current tube decreases exponentially as the distance of this tube from the axial tube along the  $z$  axis increases.

These two factors clearly localize the tunnel current to a small region around the  $z$  axis and the smallness in the lateral spread of this region determines the lateral resolution of the STM. To obtain an estimate of lateral resolution we plot  $\chi$  versus  $\rho_f$  [Fig. 3(b)]. Since  $\chi=0.5$  at  $\rho_f \approx 1.7 \text{ \AA}$ , the lateral resolution of the model chosen is of the order of  $3.4 \text{ \AA}$  when the tip has a diameter of  $10 \text{ \AA}$ .

## V. CONCLUSION

Although the above analysis, being semiclassical, does not have the rigor required for a complete analysis of the tunneling problem, it provides a picture of the tunnel-current density in a very direct way, and reasonable quantitative conclusions can be drawn from it. The special potential distribution in STM geometry obviously is responsible for the bunching of tunnel current just below the tip, thereby leading to high lateral resolution. The method we have adopted can give the tunnel-current distribution for any shape and form of the potential barrier.

We have not connected the currents to the surface electronic properties of the tip and the sample. To obtain the actual tunnel current account must be taken of the fact that the strength of the current will be proportional to the available number of electrons at the tip, and also the available number of states at the surface into which the electrons can go, i.e., to the densities of states of the electrons at the surface and at the tip energy  $E$ . Inclusion of this feature would lead to the sort of formula for the tunneling current given by Bardeen.<sup>12</sup> However, we have not considered this aspect here, our main interest being the study only of the tunnel-current distribution relative to the axial current, assuming uniform emission at each point on the surface of the tip in a direction normal to it. Our analysis supplements the other theories of STM (Refs. 13–15) which discuss the problem in terms of the total tip current and its dependence on the tip-sample separation distance and the local electronic densities of states on the sample surface and the tip.

\*Permanent address: 25 Pavonia Street, Rivett, A.C.T. 2611, Australia.

<sup>1</sup>G. Binnig, H. Rohrer, Ch. Berber, and E. Weibel, Phys. Rev. Lett. **49**, 57 (1982).

<sup>2</sup>C. F. Quate, Phys. Today **39**(8), 26 (1986).

<sup>3</sup>R. Ring, J. O. Rasmussen, and H. Massmann, Fiz. Elem. Chastits. At. Yadra **7**, 916 (1976) [Sov. J. Part. Nucl. **7**, 366 (1976)].

<sup>4</sup>W. H. Miller, J. Chem. Phys. **55**, 3146 (1971).

<sup>5</sup>W. H. Miller and T. F. George, J. Chem. Phys. **56**, 5668 (1972).

- <sup>6</sup>W. H. Miller, *J. Chem. Phys.* **62**, 1899 (1975).
- <sup>7</sup>M. Yu. Sumetskii, *Zh. Eksp. Tekh. Fiz.* **54**, 2227 (1984) [*Sov. Phys.—Tech. Phys.* **29**, 1305 (1984)].
- <sup>8</sup>A. S. Davydov, *Quantum Mechanics*, 2nd ed. (Pergamon, Oxford, 1976), Chap. III.
- <sup>9</sup>P. L. Kapur and R. Peierls, *Proc. R. Soc. London, Ser. A* **163**, 606 (1937).
- <sup>10</sup>L. D. Landau and E. M. Lifshitz, *Quantum Mechanics—Nonrelativistic Theory* (Pergamon, Oxford, 1958), Chap. VII.
- <sup>11</sup>J. Mahanty and M. T. Michalewicz, *Austral. J. Phys.* **40**, 413 (1987).
- <sup>12</sup>J. Bardeen, *Phys. Rev. Lett.* **6**, 57 (1961).
- <sup>13</sup>J. Tersoff and D. R. Hamann, *Phys. Rev. B* **31**, 805 (1985).
- <sup>14</sup>E. Stoll, A. Baratoff, A. Selloni, and P. Carnevali, *J. Phys. C* **17**, 3073 (1984).
- <sup>15</sup>T. E. Feuchtwang, P. H. Cutler, and N. M. Miskovsky, *Phys. Lett.* **99A**, 167 (1983).